catalysts

MDPI

Article

Renewable Diesel Production over Mo-Ni Catalysts Supported on Silica

John Zafeiropoulos [1], George Petropoulos [1], Eleana Kordouli [1,2,*], Labrini Sygellou [3], Alexis Lycourghiotis [2] and Kyriakos Bourikas [1,*]

[1] School of Science and Technology, Hellenic Open University, Parodos Aristotelous 18, 26335 Patras, Greece; jzafeirop@eap.gr (J.Z.); g.s.petropoulos@gmail.com (G.P.)
[2] Department of Chemistry, University of Patras, 26504 Patras, Greece; alycour@upatras.gr
[3] Foundation of Research and Technology, Institute of Chemical Engineering Science (FORTH/ICE-HT), Stadiou Str. Platani, 26500 Patras, Greece; sygellou@iceht.forth.gr
* Correspondence: ekordouli@upatras.gr (E.K.); bourikas@eap.gr (K.B.); Tel.: +30-2610997143 (E.K.); +30-2610367527 (K.B.)

Abstract: Nickel catalysts promoted with Mo and supported on silica were studied for renewable diesel production from triglyceride biomass, through the selective deoxygenation process. The catalysts were prepared by wet co-impregnation of the SiO_2 with different Ni/(Ni + Mo) atomic ratios (0/0.84/0.91/0.95/0.98/1) and a total metal content equal to 50%. They were characterized by XRD, XPS, N_2 physisorption, H_2-TPR, and NH_3-TPD. Evaluation of the catalysts for the transformation of sunflower oil to renewable (green) diesel took place in a high-pressure semi-batch reactor, under solvent-free conditions. A very small addition of Mo, namely the synergistic Ni/(Ni + Mo) atomic ratio equal to 0.95, proved to be the optimum one for a significant enhancement of the catalytic performance of the metallic Ni/SiO_2 catalyst, achieving 98 wt.% renewable diesel production. This promoting action of Mo has been attributed to the significant increase of the metallic Ni active phase surface area, the suitable regulation of surface acidity, the acceleration of the hydro-deoxygenation pathway (HDO), the creation of surface oxygen vacancies, and the diminution of coke formation provoked by Mo addition.

Keywords: silica; molybdenum–nickel catalysts; triglyceride biomass; selective deoxygenation; biofuels; renewable diesel

Citation: Zafeiropoulos, J.; Petropoulos, G.; Kordouli, E.; Sygellou, L.; Lycourghiotis, A.; Bourikas, K. Renewable Diesel Production over Mo-Ni Catalysts Supported on Silica. *Catalysts* **2024**, *14*, 662. https://doi.org/10.3390/catal14100662

Academic Editor: Xiaofeng Wang

Received: 2 September 2024
Revised: 17 September 2024
Accepted: 21 September 2024
Published: 24 September 2024

1. Introduction

According to the World Oil Outlook, the energy demand is expected to expand by 23% till 2045 [1]. Conversely, there is a lack of crude oil supplies and a need to continually reduce emissions of greenhouse gases by 45% by 2030 and reach net zero by 2050, to keep global warming to no more than 1.5 °C, as called for in the Paris Agreement [2]. Among other approaches, biofuels are an excellent alternative to fossil fuels, especially for the transport sector.

The first-generation biofuels appearing in the market are bioethanol and biodiesel. As they are produced from edible biomass, serious debate was provoked concerning the use of this kind of biomass for food or biofuels production. Fortunately, relevant research was performed on second-generation biofuels based on residual lignocellulosic and fatty biomass [3]. The latter can be easily transformed into drop-in biofuels by hydrotreatment, which is a well-established process coming from traditional refineries [4]. Fatty biomass hydrotreatment results in selective deoxygenation (SDO) of triglycerides and free fatty acids contained in this kind of biomass, leading to renewable diesel and sustainable aviation fuel (SAF), preserving the side carbon chains upon oxygen removal [5–7]. SDO proceeds via decarboxylation ($deCO_2$), decarbonylation (deCO), and the hydrodeoxygenation (HDO) of fatty acids, fatty aldehydes, and alcohols produced by hydrogenolysis/hydrogenation of

initial fatty biomass at relatively mild conditions (temperatures 240–360 °C and H_2 pressure 10–80 bar) [6,8].

In existing biorefineries, the production of renewable diesel, the so-called hydrotreated vegetable oil (HVO), has developed rapidly. HVO production can proceed through either the co-process with petroleum fractions [9] or the stand-alone process [10]. It is important to note that despite the higher capital expenditure and implementation difficulty compared to co-processing or biodiesel (Fatty Acid Methyl Esters, FAME) production from esterification, all companies have decided to invest in pure HVO production plants instead of trying co-processing. This is because, in the long run, pure HVO production offers more possibilities as it can be used on its own as drop-in or jet fuel; it can also be blended with petro-diesel to improve its parameters in any proportion, compared with FAME that can only achieve 5% blends [11].

Both methods are based on the hydrotreatment of natural triglycerides to remove oxygen selectively. In the case of a stand-alone process, noble-metal-supported catalysts [12], as well as conventional transition-metal-sulfide-supported catalysts (NiMo, CoMo, and NiW) [12–15], have been studied and found to be very reactive and selective. However, the economic feasibility and durability of the noble metal catalysts for large-scale application are questionable. Conversely, sulfide catalysts need a sulfur compound in the feed to preserve their activity, which inevitably contaminates the final product and complicates the process [16,17].

In light of the above discussion, for the last decade the focus of research has been directed to the development of less expensive and more effective sulfur-free transition metal catalysts [6,8,16,18,19]. Nickel catalysts seem to be the most promising for the title reaction because of their catalytic performance, as well as the abundance and low cost of this metal [8,20].

Both the SDO activity and the selectivity of the metallic nickel catalysts are determined by three important parameters. The first one is the magnitude of nickel active surface, ensured by preparing supported catalysts with high nickel concentration well dispersed on highly specific surface area supports. The second is the selection of the support. As already mentioned, the support should exhibit high surface area, combined with mesoporosity, balanced acidity, good supporting properties, and stability under the reaction conditions [6–8,18,21–23]. The third parameter determining the nickel catalysts' performance for SDO reactions is the selection of a suitable promoter [8,19,24].

In a previous work we have demonstrated that silica is a suitable support for SDO Ni catalysts [25]. Conversely, a very recent systematic review of the literature about the role of promoters in metallic nickel catalysts used for green diesel production identified molybdenum as the most effective promoter among several others [24]. Actually, it is better from a carbon utilization perspective since it facilitates the HDO route in comparison with the monometallic nickel catalysts, which favor the deCO route. In addition, it enhances the production of green diesel hydrocarbons due to a synergy with Ni, which appeared on bimetallic catalysts. Moreover, molybdenum may reduce methanation by inhibiting C-C bond hydrogenolysis. In view of the above, a lot of research has been done on catalysts with different nickel–molybdenum compositions, supported on different materials, prepared using different methods, and tested in various feedstock and experimental conditions [24]. To the best of our knowledge, there is not a previous systematic study of the MoNi/SiO_2 catalysts in the literature. Thus, in the present study, we examined for the first time the promoting action of Mo in Ni/SiO_2 catalysts with 50 wt.% loading of active metals, trying to determine the optimum synergistic $\frac{Ni}{Ni+Mo}$ atomic ratio. For this, adopting the wet co-impregnation method, we prepared a series of MoNi/SiO_2 catalysts with various $\frac{Ni}{Ni+Mo}$ atomic ratios. These catalysts were evaluated for the SDO of sunflower oil (SO) under solvent-free conditions, SO volume to catalyst mass equal to 100 mL/g, in a semi-batch reactor working at 310 °C, 100 mL/min H_2 flow, and 4 MPa total pressure. SO was selected as a model triglyceride feed. The catalysts were thoroughly characterized by various

physicochemical methods (N_2 physisorption, XRD, CO chemisorption, XPS, H_2-TPR, NH_3-TPD, and TGA) to link the catalysts' performance with their physicochemical properties.

2. Results and Discussion

2.1. Catalysts

The catalysts studied in this article were prepared by wet co-impregnation of the SiO_2 support with different $\frac{Ni}{Ni+Mo}$ atomic ratios (0/0.84/0.91/0.95/0.98/1). The catalysts were labeled as 0MoSi, 0.84MoNiSi, 0.91MoNiSi, 0.95MoNiSi, 0.98MoNiSi, and 1NiSi. We have focused our attention on high values of this ratio according to our previous results concerning MoNi catalysts supported on other supports (Al_2O_3 [26] and TiO_2 [27]).

Catalysts' Characterization

Textural properties of catalysts were determined by applying the method of N_2 physisorption at −195.8 °C. The corresponding isotherms (Figure S1) revealed that both catalysts and silica supported display IV-type nitrogen adsorption–desorption isotherms with a characteristic H4 hysteresis loop, indicating that all samples were mainly mesoporous materials. This was also evident in the pore-size distribution curves shown in Figure 1.

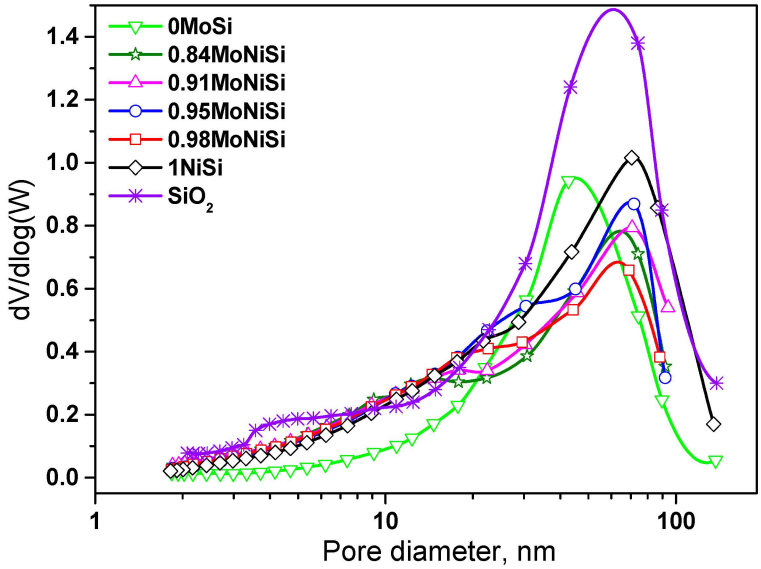

Figure 1. Pore-size distribution curves of the support and catalysts.

Table 1 shows the chemical composition of the catalysts studied and the values of BET specific surface area (SSA), BJH adsorption cumulative volume of pores (PV), BJH desorption mean pore diameter (MPD), mean crystal size of metallic nickel phase ($MCS_{Ni}{}^0$) determined by XRD, and the amount of chemically adsorbed CO on the catalysts' surface (COchem) used as a measure of catalysts' active surface. Examination of the SSA values shows that the deposition of active components on a silica surface provoked their diminution from 192 m^2g^{-1} of SiO_2 to about 126 m^2g^{-1} in cases of MoNi and Ni catalysts, while this diminution was larger in the case of a 0MoSi catalyst (77 m^2g^{-1}), indicating that MoNi and Ni phases are much better dispersed on the SiO_2 surface than Mo alone. As for the PV values, the deposition of active components provoked a slight decrease, indicating that their particles block preferentially the small mesopores. This is certified by Figure 1, which presents the pore-size distribution curves of the samples. The preferential blockage of small mesopores led to an increase of the MDP values of 0MoSi, 0.98MoNiSi, and 1NiSi, showing that in these cases bigger particles of the deposited phases were formed. In contrast, the MPD values were lower in the cases of 0.84MoNiSi, 0.91MoNiSi, and 0.95MoNiSi, showing

that the increased Mo content results in smaller particles of deposited phases well dispersed on a silica surface.

Table 1. Composition, textural, and structural characteristics of the catalysts.

Catalyst	Composition (wt.%)	SSA (m^2/g)	PV (cm^3/g)	MPD (nm)	$MCS_{Ni}{}^0$ (nm) [1]	COchem (μmole g^{-1})
SiO_2	-	192	0.97	21.6	-	-
0MoSi	50% Mo	77	0.54	27.5	-	-
0.84MoNiSi	12% Mo; 38% Ni	125	0.60	17.9	5.9	213.55
0.91MoNiSi	7% Mo; 43% Ni	126	0.68	19.5	5.8	228.41
0.95MoNiSi	4% Mo; 46% Ni	129	0.64	19.1	5.4	414.76
0.98MoNiSi	2% Mo; 48% Ni	128	0.76	22.3	7.1	371.80
1NiSi	50% Ni	124	0.72	22.1	11.7	164.96

[1] from XRD peak at 2theta 51.8° applying Scherrer's equation.

Figure 2 shows the XRD patterns of the fresh reduced catalysts studied before the reaction. In all cases, no peak that could be attributed to the SiO_2 support was observed, confirming its amorphous structure. For all bimetallic catalysts as well as for the 1NiSi catalyst, we could distinguish the dominant phase of metallic nickel at 2theta 44.6, 51.8, and 76.3°, corresponding, respectively, to the (111), (200), and (220) crystal planes of Ni^0 (JCPDS no. 03-1051). In all these cases, there were also peaks at 2theta 37.3, 43.3, and 62.8°, which corresponded, respectively, to the (111), (200), and (220) crystal planes of NiO (JCPDS no. 47-1049). Peaks of Ni phases seemed to be more intense and sharper for the monometallic 1NiSi catalyst, indicating that molybdenum enhances the dispersion of Ni.

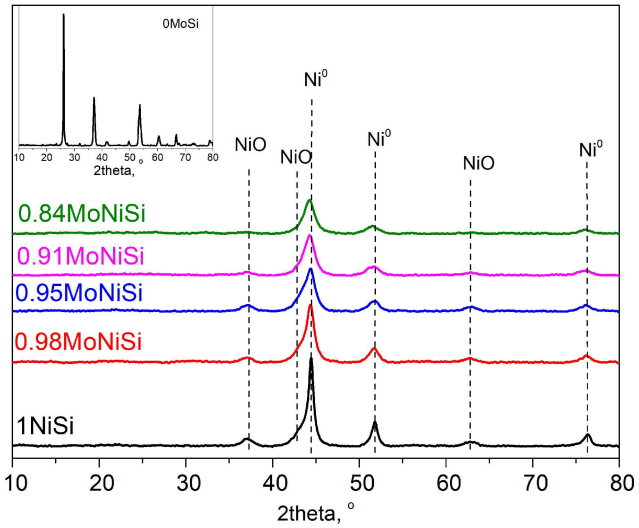

Figure 2. XRD patterns of the catalysts. The inner picture is the diffraction pattern of 0MoSi catalyst.

Conversely, the monometallic catalyst 0MoSi produced peaks of molybdenum oxide (MoO_2) at 2theta 25.8, 36.8, 53.4, 60.2, and 66.5° (JCPDS no. 78-1072). It seems that upon the activation step (reduction) of the catalysts, a reduction of Mo^{6+} to Mo^{4+} took place. In addition, we can observe that the above peaks are absent from the XRD patterns of bimetallic catalysts, a fact that can be attributed either to the small percentage of this phase or to its high dispersion.

The XRD peak at 2theta equal to 51.8° was chosen to calculate the mean size of metallic Ni crystallites ($MCS_{Ni}{}^0$) by Scherrer's equation, and the values are presented in Table 1. It can be observed that the $MCS_{Ni}{}^0$ of bimetallic catalysts were close to 6 nm, while the $MCS_{Ni}{}^0$ of monometallic catalyst 1NiSi was almost double (11.7 nm). The above difference indicates that molybdenum improves the formation of small Ni^0 crystallites in bimetallic

catalysts in comparison to the monometallic one, confirming the above statement that Mo enhances the dispersion of Ni. This effect has been also found on other supports (e.g., Al_2O_3 [28], TiO_2 [27], ZrO_2 [29], and biochar [30]). The smallest value (5.4 nm) among the bimetallic catalysts appeared for the 0.95MoNiSi sample.

The increase of nickel phase dispersion induced by XRD results was confirmed by the CO chemisorption results (Table 1). Indeed, the corresponding value increased over the bimetallic catalysts following a volcano-type trend with a maximum value over that of the 0.95MoNiSi catalyst. This indicates that this catalyst exhibits the highest active surface area, and it is expected to be the most active of the studied series.

In order to choose the appropriate reduction temperature to activate the catalysts prior to the reaction, as well as to infer the chemical interaction between supported phases (Ni and Mo phases) and SiO_2 support, H_2-TPR experiments were performed. Figure 3a shows the H_2-TPR profiles of the samples calcined at 400 °C for 2 h. The monometallic catalyst 0MoSi (inner graph of Figure 3a) exhibited two main reduction regions: the first one between 400 and 600 °C, with a maximum at 565 °C, and a second region at temperatures between 650 °C and 950 °C, consisting of a multiple reduction band. The first reduction region corresponded to the reduction of oxo-molybdate species from Mo^{6+} to Mo^{4+} [31]. This finding explains the existence of MoO_2 crystallites in the 0MoSi catalyst reduced at 400 °C for 2.5 h detected by XRD analysis (Figure 2). The second region indicated the further gradual reduction of Mo^{4+} to Mo^0 [32,33]. Such reduced species were not detected in this catalyst by XRD, in agreement with the fact that the activation (reduction) temperature was sufficiently lower.

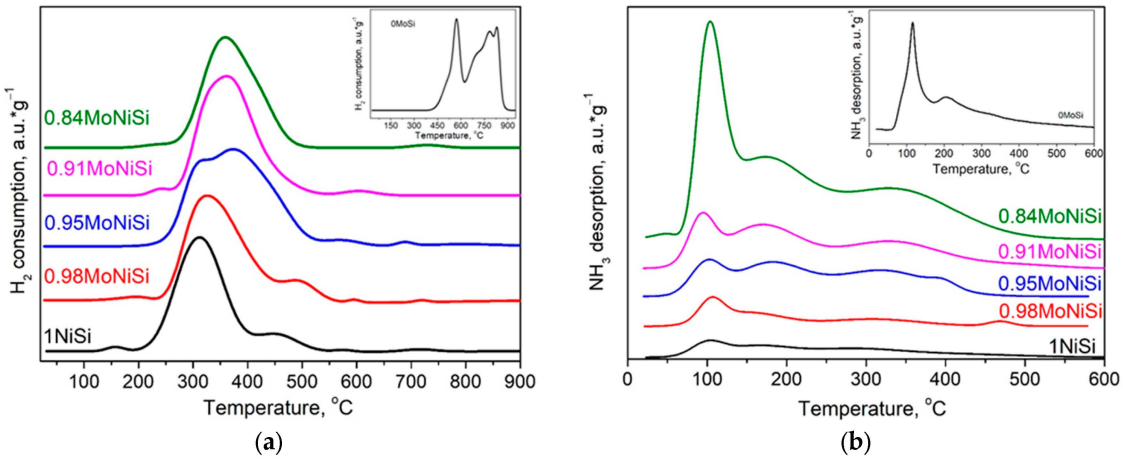

Figure 3. (**a**) H_2-TPR; (**b**) NH_3-TPD profiles of catalysts.

Inspection of the H_2-TPR profile of the monometallic 1NiSi catalyst showed three reduction peaks, with maxima at temperatures 160, 310, and 450 °C. The low temperature reduction peak was attributed to the reduction of free NiO and NiO species weakly interacting with the silica support to Ni^0. The peak with maximum at 310 °C was assigned to the reduction of well-dispersed NiO species interacting more strongly with the support. Finally, the peak with maximum at 450 °C corresponded to the reduction of NiO species incorporated in SiO_2 support matrix [34]. The H_2-TPR profile of the bimetallic samples showed the disappearance of the first reduction peak and a shift of the high temperature reduction peaks to higher temperatures. Moreover, a careful observation of the H_2-TPR curves revealed that the total amount of hydrogen consumed increased with the Mo content up to the 0.95MoNiSi catalyst. Taking into account that this catalyst has the higher nickel dispersion (XRD and CO chemisorption results (Table 1)), it seems that the smaller NiO nanoparticles are more reducible, probably because they are more accessible to hydrogen. Thus, the presence of Mo-oxo species in a small quantity not only improves the dispersion of NiO but also facilitates its reduction to metallic nickel. The addition of

more Mo (0.91MoNiSi and 0.84MoNiSi samples) considerably decreased the nickel dispersion (XRD and CO chemisorption results (Table 1)), rendering NiO less accessible to hydrogen and thus more difficult to be reduced. This was evident in the H_2-TPR profile, since the 0.84MoNiSi sample had the bigger shift in the reduction peak and the smaller hydrogen consumption, exhibiting thus the strongest anti-reduction properties. In the bimetallic catalysts, the peak assigned to $MoO_3 \rightarrow MoO_2$ reduction and expected to appear at a temperature region between 400 to 600 °C was overlapped by the reduction peak of well-dispersed NiO. Reduction peaks associated with the reduction $Mo^{4+} \rightarrow Mo^0$ were not observed in the TPR profiles of the bimetallic catalysts. This is probably due to the low Mo content and/or to the strong interaction of Mo-oxo species with the support in the bimetallic catalysts.

NH_3-TPD profiles of the catalysts are displayed in Figure 3b. NH_3 desorbed at temperatures < 250 °C, 250–450 °C, and >450 °C were assigned to weak, moderate, and strong acidic sites, respectively [35]. All catalysts exhibited peaks in temperatures lower than 450 °C, indicating the presence of weak and moderate acid sites mainly. The molybdenum addition increased the total acidity of bimetallic catalysts, without creating strong acid sites, and changed their distribution. More precisely, a small Mo amount mainly favored the creation of moderate acid sites (see TPD curves of 0.98MoNiSi, 0.95MoNiSi, and 0.91MoNiSi catalysts). This trend was reversed in the case of a 0.84MoNiSi catalyst, where a high population of weak acid sites was formed and the corresponding NH_3-TPD curve approached that of a monometallic 0MoSi catalyst (inner graph of Figure 3b).

The chemical state and surface composition of fresh activated catalysts were studied by X-ray photoelectron spectroscopy (XPS). Representative XPS Ni2p and Mo3d core-level spectra of the 0.95MoNiSi catalyst are shown in Figure 4. The Ni $2p_{3/2}$ core level spectra of all catalysts were deconvoluted using a program, which included Gaussian/Lorentzian distributions, and each Ni $2p_{3/2}$ profile was resolved in two components: ca. 852.8 and 855.8 eV. The former peak was attributed to the Ni^0 species, whereas the nearly symmetric peak appearing at binding energy of ~856 eV, accompanied by a shakeup satellite structure at ca 862.0 eV, was indicative of the existence of Ni^{2+} species.

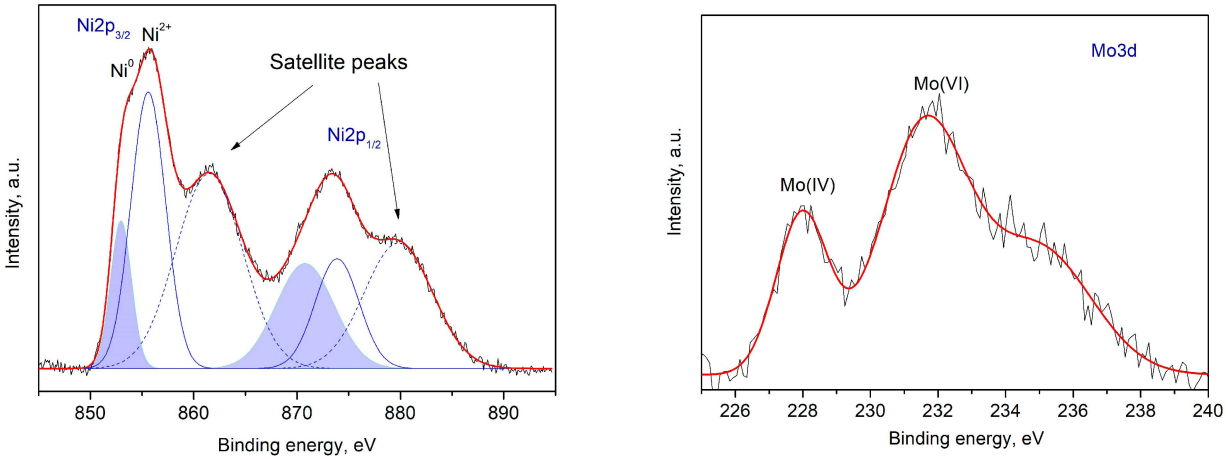

Figure 4. (**a**) Ni2p; (**b**) Mo3d core-level XPS spectra recorded for the 0.95MoNiSi catalyst.

The identification of the Mo oxidation state by XPS technique was based on the binding energies of the Mo ($3d_{5/2}$, $3d_{3/2}$) spin-orbit components. Peak deconvolution revealed two partially overlapped Mo 3d doublets with BE of ~228 eV characteristic of Mo^{4+} (MoO_2) and of ~232 eV corresponding to Mo^{6+} species (MoO_3) [36]. The first ones (reduced Mo-species) created oxygen vacancies on the catalysts surface [37]. The area of the first peak

indicated a significant amount of surface-reduced Mo (Mo(IV)), thus creating a considerable concentration of oxygen vacancies.

Based on the XPS results, the surface composition of the catalysts was calculated, and the corresponding values are summarized in Table 2. These values revealed that the main fraction of the surface nickel was in the oxide form even after activation (reduction at 400 °C). This fraction seemed to increase with the Mo addition, confirming the reduction retardation observed via H_2-TPR and XRD results. Table 2 shows also that the $\frac{Ni}{Ni+Mo}$ atomic ratio on the catalysts surface was too close to the theoretical one targeted upon catalysts preparation. This was another indication that good dispersion and uniform surface distribution of the supported phases was achieved.

Table 2. Surface composition of the reduced catalysts determined by XPS.

Catalyst	% Ni Components		$\frac{Ni}{Ni+Mo}$
	%Ni^0	%NiO	
0MoSi	-	-	0
0.84MoNiSi	28.1	71.9	0.81
0.91MoNiSi	30.3	69.7	0.90
0.95MoNiSi	30.0	70.0	0.94
0.98MoNiSi	29.9	70.1	0.97
1NiSi	33.0	67.0	1

2.2. Catalysts' Performance

The catalysts were evaluated for the Selective Deoxygenation (SDO) of natural triglycerides, using commercial sunflower oil (SO) as a model triglyceride feed. The experiments took place in a semi-batch reactor using 1 g of catalyst, 100 mL of SO (solvent free), 40 bar pressure, H_2 flow of 100 mL/min, temperature 310 °C, and stirring 2000 rpm. The reaction over each catalyst studied was followed for 9 h.

Figure 5 presents the liquid phase composition obtained at the end of each experiment. This figure shows that all bimetallic catalysts as well as the monometallic nickel catalyst achieved complete conversion of SO. In contrast, the molybdenum monometallic catalyst (0MoSi) achieved only 66% SO conversion. Inspection of Figure 5 reveals that the yield of hydrocarbons (n-alkanes) rose with the Mo content of bimetallic catalysts, resulting in the highest hydrocarbon concentration of 98 wt.% in the liquid phase, obtained using the 0.95MoNiSi catalyst, and then decreased as the Mo content increased further. The promoting action of Mo-oxo species to the Ni active phase supported on SiO_2 was manifested as all bimetallic catalysts resulted in higher values of hydrocarbon yield in comparison to the monometallic 1NiSi (with 66 wt.%) and 0MoSi (with 1 wt.%). The above presented results are also perfectly supported by the physicochemical characteristics of the best bimetallic catalyst, 0.95NiMoSi, which combined the following: (i) high value of specific surface area (129 m^2/g), (ii) increased dispersion of the metallic nickel with small $MCS_{Ni}{}^0$ (5.4 nm) (XRD, CO chemisorption and XPS), (iii) a balanced moderate acidity (NH_3-TPD) (factors that play a key role in the SDO of natural triglycerides into green diesel), and (iv) considerable surface concentration of reduced Mo species (rich in oxygen vacancies), causing a synergistic mechanism with the neighboring metallic nickel sites, as reported in the literature [24,27] (see details below). This study reveals that only a small amount of molybdenum is needed to express its promoting action in Ni-based catalysts supported on SiO_2. This finding is common for such catalysts supported on other supports (Al_2O_3 [28], TiO_2 [27], ZrO_2 [29], and biochar [30]).

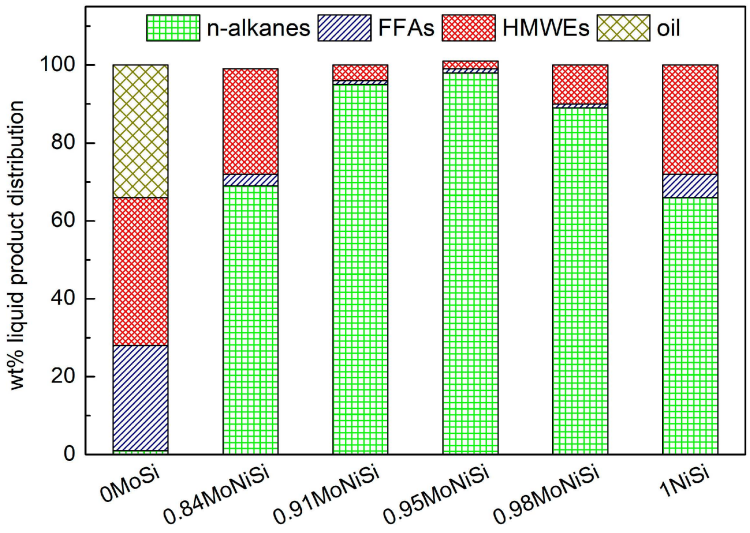

Figure 5. Liquid products' distributions obtained upon the transformation of SO over the catalysts studied. Reaction conditions: SO/catalyst ratio = 100 mL/g, pressure = 40 bar, temperature = 310 °C, H_2 flow rate = 100 mL/min, and time = 9 h.

It is well-known that Ni-based catalysts accelerate mainly the deCOx (deCO + deCO$_2$) pathways in relation with the HDO one upon SDO processing [6,8,12,19]. To clarify this point in the case of our catalysts, we determined, in the liquid phase obtained in each catalytic test, the concentration of hydrocarbons with an odd number of carbon atoms (C15 + C17), being products of the deCOx route, and that of hydrocarbons with an even number of carbon atoms (C16 + C18), which are products of HDO route. Figure 6 presents the corresponding results. It can be seen that an Mo addition in Ni catalysts accelerated both deCOx and HDO pathways, favoring somewhat more the latter. Indeed, although HDO products were not detected in the case of 0MoSi catalyst, their concentration in the liquid phase increased with the increase of Mo content in the bimetallic catalysts. This is more evident by calculating the HDO/deCOx products' concentration ratio (1NiSi: 0.1, 0.98MoNiSi: 0.12, 0.95MoNiSi: 0.17, 0.91MoNiSi: 0.20, and 0.84MoNiSi: 0.35).

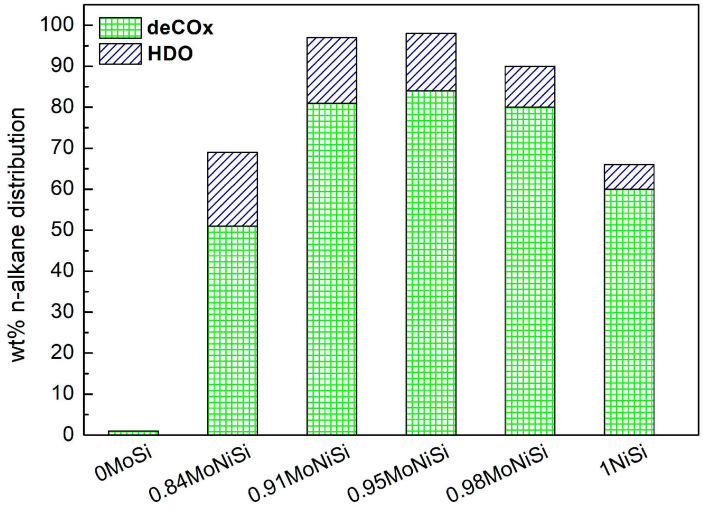

Figure 6. Composition of the liquid product in n-alkanes with odd (deCOx) and even (HDO) numbers of carbon atoms, obtained over the catalysts studied for a reaction time equal to 9 h. Reaction conditions: SO/catalyst ratio = 100 mL/g, pressure = 40 bar, temperature = 310 °C, H_2 flow rate = 100 mL/min, and time = 9 h.

Kinetic results concerning the most active catalyst of this series are presented in Figure 7. These results show that complete conversion of SO was achieved even after the first hour of catalytic testing. However, the maximum hydrocarbons production was achieved after 9 h. This is because intermediate products like free fatty acids (FFAs) and high molecular weight esters (HMWEs) were formed according to the well-established SDO mechanism describing the solvent-free process over Ni-based catalysts [8,12,24]. This mechanism predicts that upon triglycerides' hydrotreatment, they are easily saturated and then hydrolyzed to FFAs. The latter are either decarboxylated towards hydrocarbons or reduced to aldehydes. Then, aldehydes are reduced to the corresponding alcohols. The alcohols could be dehydrated and hydrogenated to hydrocarbons with the same number of carbon atoms or to react with FFAs (esterification) to produce HMWEs. The kinetic results, presented in Figure 7, confirmed the above-discussed mechanism, showing that HMWEs are the most difficultly deoxygenated intermediates.

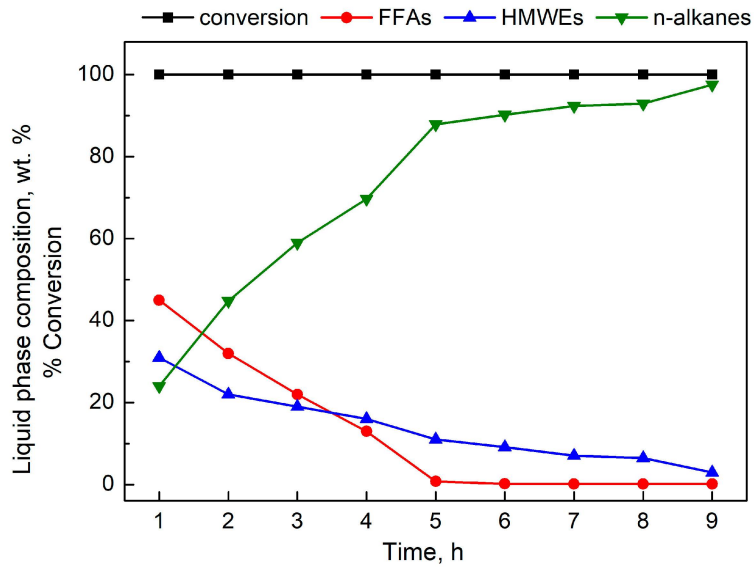

Figure 7. Kinetics of transformation of SO over the catalyst 0.95MoNiSi. The composition of the liquid phase for a given time in hydrocarbons (n-alkanes), free fatty acids (FFAs), and high molecular weight esters (HMWEs) at various times is illustrated. Reaction conditions: SO/catalyst ratio = 100 mL/g, pressure = 40 bar, temperature = 310 °C, and H_2 flow rate = 100 mL/min.

The reduced Mo-species found in the bimetallic catalysts (see XPS results) played a crucial role in the above-described kinetics. These species facilitated the observed activity and selectivity to hydrocarbons because to their abundance of oxygen vacancies. More specifically, a synergy was observed between the oxygen vacancies on the surface of Mo species with oxidation states below six and the adjacent metallic Ni sites [24,27]. Actually, the intermediate FFAs are adsorbed onto the aforementioned sites via the oxygen atom of the C-OH group, therefore activating the C-O bond. The hydrogen atoms generated from the dissociative adsorption of H_2 on metallic nickel sites attacked this bond, resulting in the conversion of the FFAs to their respective fatty aldehydes. Consequently, the most time-consuming reaction of the SDO mechanism accelerated. Furthermore, the aldehydes produced were adsorbed onto oxygen vacancies via the oxygen atom of the C=O bond, which was activated, hence accelerating the reduction of aldehydes to their corresponding fatty alcohols, elucidating the role of Mo in promoting the HDO pathway of the SDO process in relation with the deCOx pathway (see Figure 6).

Going from the fresh to the used catalysts, we have to mention that reusability tests were performed over the most active catalyst of the series. More precisely, after the first catalytic run, the liquid phase was removed from the reactor and replaced by 100 mL of fresh SO. The catalyst was washed with hexane several times to remove any liquid organic

substances entrapped in its pores, and then it was dried under a vacuum. Then, the catalyst was added to the reactor and a new run was performed following the same protocol as the first time. The procedure was repeated two more times. Figure 8 shows the results obtained.

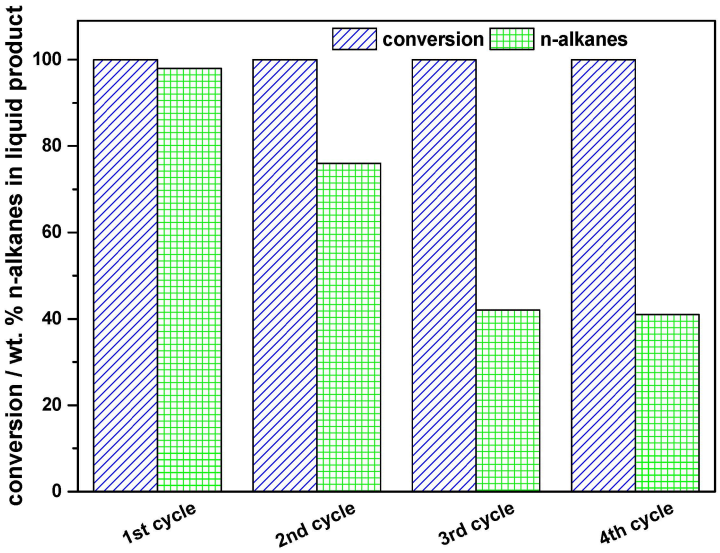

Figure 8. Reusability study of the 0.95MoNiSi catalyst towards hydrocarbons concentration of the liquid phase. Reaction conditions: SO/catalyst ratio = 100 mL/g, pressure = 40 bar, temperature = 310 °C, H_2 flow rate = 100 mL/min, and reaction time = 9 h.

Inspection of this figure indicates that the 0.95MoNiSi catalyst maintained substantial performance for renewable diesel production (~40 wt.%) even after four cycles of reaction. The harsh reaction conditions used in our catalysts' evaluation tests (solvent-free, SO/catalyst ratio = 100 mL/g, pressure = 40 bar, temperature = 310 °C, and H_2 flow rate = 100 mL/min) simulated corresponding tests in a fixed-bed reactor working with LHSV equal to 11.1 h^{-1}. As in industrial processes LHSV values 1–2 h^{-1} are adopted, 0.95MoNiSi catalyst could be active enough at least for 200–400 h on stream. However, for an industrial application of the catalyst, more effort is required in the future in order to increase the durability of the catalyst.

In an attempt to investigate the reasons for the catalysts' deactivation, the 0.95MoNiSi was characterized by N_2 physisorption, XRD, and TGA analysis after the first activity test. The results obtained are summarized in Table 3 and Figure 9. Table 3 reveals a reduction in SSA and PV values in the spent catalyst. These results could be attributed in some plugin of the small mesopores by coke deposition in accordance with the pore-size distribution curves (Figure 9a). The latter shows that after the catalytic run, some new pores in macropores region were formed. These were probably interparticle pores created among the catalyst's particles that stuck with the deposited coke. The plugin of small mesopores was responsible for the increased MPD value observed in the spent catalyst.

Table 3. Textural and structural characteristics of the fresh and spent 0.95MoNiSi catalysts.

Catalyst	SSA (m^2/g)	PV (cm^3/g)	MPD (nm)	$MCS_{Ni}{}^0$ (nm)
fresh 0.95MoNiSi	129	0.64	19.1	5.4
spent 0.95MoNiSi [1]	107	0.44	26.3	16.6

[1] The spent catalyst was washed with n-hexane and dried at 110 °C before characterization.

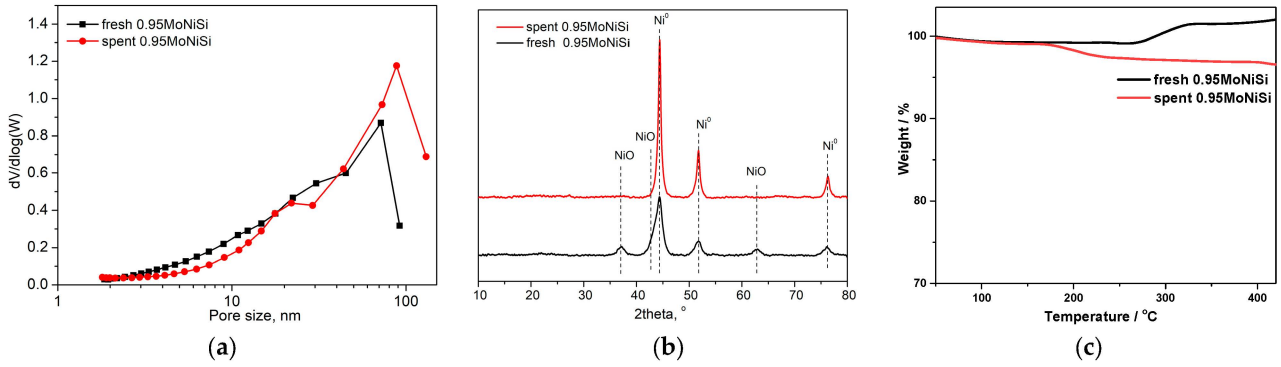

Figure 9. (**a**) Pore-size distribution curves, (**b**) XRD patterns, and (**c**) TGA curves of the fresh and spent 0.95MoNiSi catalysts.

According to Figure 9b, which presents the XRD patterns of the fresh and spent 0.95MoNiSi catalysts, it is obvious that the reaction conditions adopted (310 °C, 40 MPa, and 100 mL/min H_2 flow) led to a complete reduction of NiO and to the increase of $MCS_{Ni}{}^0$ (Table 3), confirmed by the intensity and the sharpness of the corresponding XRD peaks.

In order to determine the coke amount deposited on catalyst surface upon catalytic test, TG analyses of fresh and spent catalyst were performed. Figure 9c reveals that upon the TGA experiment on the fresh catalyst, a 2% weight gain was observed. This could be attributed to the transformation of Ni^0 to NiO. In contrast, a 3% weight loss was observed upon TGA of the spent catalyst. Thus, a difference of 5% weight loss could be attributed to the combustion of deposited coke. In this point, it should be noted that the coke deposited on 1NiSi was 15%. This shows another favoring action of Mo addition to the Ni catalyst used for SDO of fatty biomass.

3. Materials and Methods

3.1. Materials

The following reagents were used in the preparation of the catalysts: $Ni(NO_3)_2$ $6H_2O$ (Alpha Aesar, Peristeri, Greece, analytical grade 98%), $(NH_4)_6Mo_7O_{24}$ $4H_2O$, (Carlo Erba Reagenti, Emmendingen, Germany, analytical grade 81.6–83.8%), ethylenediamine (Sigma-Aldrich, Marousi, Greece, analytical grade > 99.5%), acetone (Sigma-Aldrich, analytical grade > 99.5%), NH_4NO_3 (Riedel-de Haen, Charlotte, NC, USA, 98%), Milli-Q water (Gradient), and SiO_2 (Alfa, Montgomery, AL, USA, amorphous fumed, 99.8% metal base 325 mesh). Commercial sunflower oil was purchased from the local market. The precursor salt $Ni(en)_3(NO_3)_2$ was synthesized in the lab. Experimental details are given in the Supplementary Materials file.

3.2. Catalysts' Synthesis

Following the wet impregnation method, we synthesized the MoNiSi catalysts with different $\frac{Ni}{Ni+Mo}$ atomic ratios (0/0.84/0.91/0.95/0.98/1), keeping the total amount of deposited metals constant at 50 wt.%. Full experimental details about the synthesis protocol and the quantities of materials used (Table S1) can be found in the Supplementary Materials file.

3.3. Catalysts' Activation

The calcined samples were activated by reduction with H_2 (40 mL/min), in a fixed bed reactor, at 400 °C for 2.5 h, following a protocol adopted in a previous recent work [27]. The final catalysts are symbolized as xMoNiSi, where x represents the Ni/(Ni + Mo) atomic ratio.

3.4. Catalysts' Characterization

The catalysts were thoroughly characterized by the following: (a) N_2 physisorption, (b) X-ray diffraction (XRD), (c) temperature-programmed reduction with H_2 (H_2-TPR),

(d) temperature-programmed desorption of ammonia (NH_3-TPD), (e) X-ray photoelectron spectroscopy (XPS), and (f) thermogravimetric analysis (TGA). Full experimental details concerning the implementation of the techniques can be found in the Supplementary Materials file or in three recent publications [25,27,38].

3.5. Catalysts' Evaluation

The catalysts were evaluated for the green diesel production by hydrotreatment of sunflower oil, in a semi-batch reactor (300 mL, Autoclave Engineers, Erie, PA, USA), in the absence of any solvent, at 310 °C, H_2 flow rate 100 mL/min, 40 bar total pressure, oil volume to catalyst mass ratio 100 mL/g, and stirring rate 2000 rpm, for 9 h.

The liquid phase in the reactor was followed with the reaction time by withdrawing 1 mL aliquots at one-hour intervals. Their compositions were determined by gas chromatography (Shimadzu GC-2010 plus, Kyoto, Kyoto, equipped with FID and a ZB-5HT column (INFERNO, ZEBRON, Torrance, CA, USA, l = 30 m, d = 0.52 mm, and tf = 0.10 μm)). Details of the chromatographic analysis have been given elsewhere [34].

4. Conclusions

The main conclusions drawn from this study are as follows:

MoNi catalysts supported on silica exhibited excellent performance in converting fatty biomass to hydrocarbons in the diesel range. The Mo-promoting action in the nickel catalysts was attributed to the significant increase of the Ni^0 active phase surface area, the suitable regulation of surface acidity, the acceleration of the HDO pathway, the creation of surface oxygen vacancies, and the diminution of coke formation provoked by the Mo addition.

A very small amount of Mo (synergistic $\frac{Ni}{Ni+Mo}$ atomic ratio equal to 0.95) proved to be enough for significantly enhancing the catalytic performance of SiO_2-supported Ni catalysts, achieving 98 wt.% renewable diesel production from sunflower oil, in a high-pressure semi-batch reactor, under solvent-free conditions.

Supplementary Materials: The following supporting information can be downloaded at: https://www.mdpi.com/article/10.3390/catal14100662/s1, Figure S1: N_2 physisorption isotherms of the support and the catalysts, Table S1: Quantities of support, nickel precursor, and molybdenum precursor used for the synthesis of the catalysts through the WI technique (xMoNiSi, where x denotes the Ni/(Ni + Mo) atomic ratio).

Author Contributions: Conceptualization, K.B. and A.L.; methodology, J.Z. and G.P.; software, E.K. and L.S.; validation, J.Z. and G.P.; formal analysis, J.Z. and L.S.; investigation, J.Z. and G.P.; data curation, J.Z. and L.S.; writing—original draft preparation, E.K.; writing—review and editing, K.B.; visualization, E.K., K.B. and A.L.; supervision, K.B.; project administration, K.B. All authors have read and agreed to the published version of the manuscript.

Funding: This research received no external funding.

Data Availability Statement: All data supporting the reported results can be found in the published article.

Conflicts of Interest: The authors declare no conflicts of interest.

References

1. Aliefendic, H.; Ban, J.; Diendorfer, C.; AlNaeimi, R.; Attaba, M. Energy demand. In *World Oil Outlook 2045*; OPEC: Vienna, Austria, 2023; Chapter 2, pp. 47–81.
2. UAE Energy Strategy 2050. Available online: https://u.ae/en/about-the-uae/strategies-initiatives-and-awards/strategies-plans-and-visions/environment-and-energy/uae-energy-strategy-2050 (accessed on 16 July 2024).
3. Padder, S.A.; Khan, R.; Rather, R.A. Biofuel generations: New insights into challenges and opportunities in their microbe-derived industrial production. *Biomass Bioenergy* **2024**, *185*, 107220. [CrossRef]
4. Gil, A.; Sancho-Sanz, I.; Korili, S.A. Progress and Perspectives in the Catalytic Hydrotreatment of Bio-Oils: Effect of the Nature of the Metal Catalyst. *Ind. Eng. Chem. Res.* **2024**, *63*, 11759–11775. [CrossRef]

5. Kubička, D.; Kubičková, I.; Čejka, J. Application of Molecular Sieves in Transformations of Biomass and Biomass-Derived Feedstocks. *Catal. Rev. Sci. Eng.* **2013**, *55*, 1–78. [CrossRef]
6. Yao, X.; Strathmann, T.J.; Li, Y.; Cronmiller, L.E.; Ma, H.; Zhang, J. Catalytic hydrothermal deoxygenation of lipids and fatty acids to diesel-like hydrocarbons: A review. *Green Chem.* **2021**, *23*, 1114–1129. [CrossRef]
7. Mahdi, H.; Bazargan, A.; McKay, G.; Azelee, N.I.W.; Meili, L. Catalytic deoxygenation of palm oil and its residue in green diesel production: A current technological review. *Chem. Eng. Res. Des.* **2021**, *174*, 158–187. [CrossRef]
8. Kordulis, C.; Bourikas, K.; Gousi, M.; Kordouli, E.; Lycourghiotis, A. Development of nickel based catalysts for the transformation of natural triglycerides and related compounds into green diesel: A critical review. *Appl. Catal. B* **2016**, *181*, 156–196. [CrossRef]
9. Yáñez, É.; Meerman, H.; Ramírez, A.; Castillo, É.; Faaij, A. Assessing bio-oil co-processing routes as CO_2 mitigation strategies in oil refineries. *Biofuels Bioprod. Biorefin.* **2021**, *15*, 305–333. [CrossRef]
10. Bezergianni, S.; Dimitriadis, A.; Karonis, D. Diesel decarbonization via effective catalytic Co-hydroprocessing of residual lipids with gas–oil. *Fuel* **2014**, *136*, 366–373. [CrossRef]
11. Seibel, J.; Wancura, J.H.C.; Mayer, F.D. Process simulation and technology prospection to the hydrotreating of vegetable oils and animal fats. *Energy Convers. Manag.* **2024**, *315*, 118811. [CrossRef]
12. Mussa, N.-S.; Toshtay, K.; Capron, M. Catalytic Applications in the Production of Hydrotreated Vegetable Oil (HVO) as a Renewable Fuel: A Review. *Catalysts* **2024**, *14*, 452. [CrossRef]
13. Coumans, A.E.; Hensen, E.J.M. A model compound (methyl oleate, oleic acid, triolein) study of triglycerides hydrodeoxygenation over alumina-supported NiMo sulfide. *Appl. Catal. B* **2017**, *201*, 290–301. [CrossRef]
14. Arora, P.; Ojagh, H.; Woo, J.; Lind Grennfelt, E.; Olsson, L.; Creaser, D. Investigating the effect of Fe as a poison for catalytic HDO over sulfided NiMo alumina catalysts. *Appl. Catal. B* **2018**, *227*, 240–251. [CrossRef]
15. Vlasova, E.N.; Bukhtiyarova, G.A.; Deliy, I.V.; Aleksandrov, P.V.; Porsin, A.A.; Panafidin, M.A.; Gerasimov, E.Y.; Bukhtiyarov, V.I. The effect of rapeseed oil and carbon monoxide on SRGO hydrotreating over sulfide $CoMo/Al_2O_3$ and $NiMo/Al_2O_3$ catalysts. *Catal. Today* **2020**, *357*, 526–533. [CrossRef]
16. Li, X.; Luo, X.; Jin, Y.; Li, J.; Zhang, H.; Zhang, A.; Xie, J. Heterogeneous sulfur-free hydrodeoxygenation catalysts for selectively upgrading the renewable bio-oils to second generation biofuels. *Renew. Sustain. Energy Rev.* **2018**, *82*, 3762–3797. [CrossRef]
17. Srifa, A.; Viriya-empikul, N.; Assabumrungrat, S.; Faungnawakij, K. Catalytic behaviors of $Ni/\gamma\text{-}Al_2O_3$ and $Co/\gamma\text{-}Al_2O_3$ during the hydrodeoxygenation of palm oil. *Catal. Sci. Technol.* **2015**, *5*, 3693–3705. [CrossRef]
18. Chen, S.; Zhou, G.; Miao, C. Green and renewable bio-diesel produce from oil hydrodeoxygenation: Strategies for catalyst development and mechanism. *Renew. Sustain. Energy Rev.* **2019**, *101*, 568–589. [CrossRef]
19. Malins, K. Synthesis of renewable hydrocarbons from vegetable oil feedstock by hydrotreatment over selective sulfur-free $SiO_2\text{-}Al_2O_3$ supported monometallic Pd, Pt, Ru, Ni, Mo and bimetallic NiMo catalysts. *Fuel* **2021**, *285*, 119129. [CrossRef]
20. Jeon, K.-W.; Gong, J.-H.; Kim, M.-J.; Shim, J.-O.; Jang, W.-J.; Roh, H.-S. Review on the production of renewable biofuel: Solvent-free deoxygenation. *Renew. Sustain. Energy Rev.* **2024**, *195*, 114325. [CrossRef]
21. Rahmawati, Z.; Santoso, L.; McCue, A.; Jamari, N.L.A.; Ninglasari, S.Y.; Gunawan, T.; Fansuri, H. Selectivity of reaction pathways for green diesel production towards biojet fuel applications. *RSC Adv.* **2023**, *13*, 13698. [CrossRef]
22. Lucantonio, S.; Di Giuliano, A.; Rossi, L.; Gallucci, K. Green Diesel Production via Deoxygenation Process: A Review. *Energies* **2023**, *16*, 844. [CrossRef]
23. Douvartzides, S.L.; Charisiou, N.D.; Papageridis, K.N.; Goula, M.A. Green Diesel: Biomass Feedstocks, Production Technologies, Catalytic Research, Fuel Properties and Performance in Compression Ignition Internal Combustion Engines. *Energies* **2019**, *12*, 809. [CrossRef]
24. Lycourghiotis, S.; Kordouli, E.; Bourikas, K.; Kordulis, C.; Lycourghiotis, A. The role of promoters in metallic nickel catalysts used for green diesel production: A critical review. *Fuel Process. Technol.* **2023**, *244*, 107690. [CrossRef]
25. Zafeiropoulos, J.; Petropoulos, G.; Kordouli, E.; Kordulis, C.; Lycourghiotis, A.; Bourikas, K. Development of nickel catalysts supported on silica for green diesel production. *Catal. Today* **2023**, *423*, 113952. [CrossRef]
26. Kordouli, E.; Sygellou, L.; Kordulis, C.; Bourikas, K.; Lycourghiotis, A. Probing the synergistic ratio of the $NiMo/\gamma\text{-}Al_2O_3$ reduced catalysts for the transformation of natural triglycerides into green diesel. *Appl. Catal. B* **2017**, *209*, 12–22. [CrossRef]
27. Petropoulos, G.; Zafeiropoulos, J.; Kordouli, E.; Sygellou, L.; Kordulis, C.; Lycourghiotis, A.; Bourikas, K. Transformation of vegetable oils into green diesel over Ni-Mo catalysts supported on titania. *Catal. Today* **2023**, *423*, 114268. [CrossRef]
28. Kordouli, E.; Pawelec, B.; Bourikas, K.; Kordulis, C.; Fierro, J.L.G.; Lycourghiotis, A. Mo promoted $Ni\text{-}Al_2O_3$ co-precipitated catalysts for green diesel production. *Appl. Catal. B* **2018**, *229*, 139–154. [CrossRef]
29. Nikolopoulos, N.; Kordouli, E.; Sygellou, L.; Bourikas, K.; Kordulis, C.; Lycourghiotis, A. Mo promoted $Ni\text{-}ZrO_2$ co-precipitated catalysts for green diesel production. *Chem. Eng. Sci.* **2023**, *270*, 118540. [CrossRef]
30. Nikolopoulos, I.; Kordouli, E.; Mourgkogiannis, N.; Karapanagioti, H.K.; Lycourghiotis, A.; Kordulis, C. Valorization of Pyrolyzed Biomass Residues for the Transformation of Waste Cooking Oil into Green Diesel. *Catalysts* **2023**, *13*, 1004. [CrossRef]
31. Zepeda, T.A.; Torres-García, N.L.; Antúnez-García, J.; Galván, D.H.; Pawelec, B.; Huirache-Acuña, R.; Díaz de León, J.N.; Alonso-Núñez, G.; Fierro, J.L.G.; Fuentes, S. Synergetic effect in $Ru_xMo_{(1-x)}S_2$/SBA-15 hydrodesulfurization catalysts: Comparative experimental and DFT studies. *Appl. Catal. B* **2019**, *251*, 143–153. [CrossRef]
32. Chary, K.V.R.; Reddy, K.R.; Kumar, C.P. Dispersion and reactivity of molybdenum oxide catalysts supported on titania. *Catal. Commun.* **2001**, *2*, 277–284. [CrossRef]

33. Liu, K.; Huang, X.; Pidko, E.A.; Hensen, E.J.M. MoO_3–TiO_2 synergy in oxidative dehydrogenation of lactic acid to pyruvic acid. *Green Chem.* **2017**, *19*, 3014–3022. [CrossRef]
34. Chagas, C.A.; Manfro, R.L.; Toniolo, F.S. Production of Hydrogen by Steam Reforming of Ethanol over Pd-Promoted Ni/SiO_2 Catalyst. *Catal. Lett.* **2020**, *150*, 3424–3436. [CrossRef]
35. Zhang, J.; Chen, T.; Jiao, Y.; Cheng, M.; Wang, L.-L.; Wang, J.-L.; Li, X.-Y.; Chen, Y.-Q. Improved activity of Ni–Mo/SiO_2 bimetallic catalyst synthesized via sol-gel method for methylcyclohexane cracking. *Pet. Sci.* **2021**, *18*, 1530–1542. [CrossRef]
36. García-Pérez, D.; Alvarez-Galvan, M.C.; Capel-Sanchez, M.C.; Blanco-Brieva, G.; Morales-delaRosa, S.; Campos-Martin, J.M.; Fierro, J.L.G. Influence of bimetallic characteristics on the performance of MoCoP and MoFeP catalysts for methyl laurate hydrodeoxygenation. *Catal. Today* **2021**, *367*, 43–50. [CrossRef]
37. Yang, C.; Wang, W.; Wang, D.; Gong, M.; Xin, Y.; Xiao, L.; Kikhtyanin, O.V.; Kubicka, D.; Wu, W. The promotion effects of MoOx species in the highly effective NiMo/$MgAl_2O_4$ catalysts for the hydrodeoxygenation of methyl palmitate. *J. Environ. Chem. Eng.* **2022**, *10*, 107761. [CrossRef]
38. Petropoulos, G.; Zafeiropoulos, J.; Kordouli, E.; Lycourghiotis, A.; Kordulis, C.; Bourikas, K. Influence of Nickel Loading and the Synthesis Method on the Efficiency of Ni/TiO_2 Catalysts for Renewable Diesel Production. *Energies* **2023**, *16*, 4333. [CrossRef]